



A four state parametric model for the kinetics of the non-photochemical quenching in Photosystem II

Joris J. Snellenburg^a, Matthew P. Johnson^b, Alexander V. Ruban^c, Rienk van Grondelle^a, Ivo H.M. van Stokkum^{a,*}

^a Institute for Lasers, Life and Biophotonics, Faculty of Sciences, VU University Amsterdam, De Boelelaan 1081, 1081 HV Amsterdam, The Netherlands.

^b Department of Molecular Biology and Biotechnology, University of Sheffield, UK

^c School of Biological and Chemical Sciences, Queen Mary University of London, UK

ARTICLE INFO

Keywords:

Fluorescence quenching analysis
Non-photochemical quenching
Parameter estimation
Time-resolved fluorescence spectroscopy

ABSTRACT

The phenomenon of non-photochemical quenching (NPQ) was studied in spinach chloroplasts using pulse amplitude modulated (PAM) fluorometry. We present a new analysis method which describes the observed fluorescence quantum yield as the sum of the product of four different states of PSII and their corresponding quantum yields. These four distinct states are PSII in the quenched or unquenched state, and with its reaction center either open or closed depending upon the reduction of the Q_A site. With this method we can describe the dynamics of the NPQ induction and recovery as well as quantify the percentage of photoinactivated RC throughout the measurement. We show that after one cycle of quenching followed by a period of recovery, approximately 8–9% of the RC are photoinactivated, after two cycles of illumination this number becomes 15–17%. The recovery from the quenching appeared with rates of $(50 \text{ s})^{-1}$ and $(1 \text{ h})^{-1}$. The new analysis method presented here is flexible, allowing it to be applied to any type of PAM fluorometry protocol. The method allows to quantitatively compare qualitatively different PAM curves on the basis of statistically relevant fitting parameters and to quantify quenching dynamics and photoinactivation. Moreover, the results presented here demonstrate that the analysis of a single PAM fluorometry quenching experiment can already provide information on the relative quantum yield of the four different states of PSII for the intact chloroplasts - something no other form of spectroscopy could provide in a single measurement.

1. Introduction

Non-photochemical quenching (NPQ) has long been in the focus of photosynthesis research [1]. Recently, the fundamental knowledge on the kinetic aspects of NPQ has been utilized in the creation of highly productive crops [2]. Therefore it is essential to create a model describing these kinetics in order to obtain key physiological parameters of Photosystem II (PSII) activity.

Pulse amplitude modulation (PAM) fluorometry is a technique which can be used to measure the fluorescence quantum yield even in the presence of actinic light [3,4], and as such can be performed in a wide range of physiological conditions. The required equipment is relatively inexpensive and can even be carried into the field [5].

The fluorescence detected by a PAM fluorometer originates from all pigment-protein complexes that absorb light at the excitation wavelength used and emit fluorescence overlapping with its detector

window (typically $\lambda > 700 \text{ nm}$). Modulation is used to ensure that the recorded signal is due to the (constant) modulated measuring light only. Any increase or decrease in the recorded signal can directly be related to changes in the fluorescence quantum yield of the different pigment protein complexes.

Theoretical models of the light dependent reactions in the thylakoid membrane can predict a PAM signal, which can be used to verify such models. The (fast) kinetics of chlorophyll fluorescence induction is described in e.g. [6–8] reviewed in [9,10] and more recently [11]. The slower processes such as NPQ and state transitions, are modelled in [12–16].

Here we start not from theory, but from the experimental data, and analyze the PAM signals of various intact chloroplasts obtained using a typical light protocol used for quenching analysis experiments [17], and quantify the dynamically changing concentrations of the different emissive species. The artificial electron acceptor methylviologen was

Abbreviations: Chl, chlorophyll; GA, glutaraldehyde; LHC, light harvesting complex; LR, light regime; NPQ, non-photochemical quenching; PAM, pulse amplitude modulation; PSI, Photosystem I; PSII, Photosystem II; RC, reaction center; SP, saturating pulse; V, devoid of zeaxanthin; Z, (enriched in) zeaxanthin

* Corresponding author.

E-mail address: ivo@few.vu.nl (I.H.M. van Stokkum).

<http://dx.doi.org/10.1016/j.bbabbio.2017.08.004>

Received 27 January 2017; Received in revised form 12 July 2017; Accepted 5 August 2017

Available online 08 August 2017

0005-2728/ © 2017 Elsevier B.V. All rights reserved.

used in this study to promptly obtain a stable level of the proton gradient, the trigger for NPQ, upon illumination. This was a simplification of an experimental scheme in order to avoid further complexity of the modelling process and therefore minimize the number of variables. In our approach we explicitly assume a discrete number of states for the contribution of PSII. It can be quenched or unquenched and switches between these extremes due to changes in the actinic light. At the same time it can be open or closed dependent on the reduction state of Q_A of the PSII RC, resulting in a total of four discrete states for PSII. Apart from PSII which dominates the signal there are other emissive species that contribute to the fluorescence quantum yield, e.g. PSI [18,19], disconnected antenna complexes such as light harvesting complex I and II (LHCI and LHCII [20] respectively). The relative concentrations and the quantum yields of different emissive species depend on the organism, growing conditions, mutations, chemical treatments, etc. We employ a parametric model which takes the light protocol and the high quality measurements as input and aims to describe the data up to the noise level, in order to extract all the information available. The method is flexible enough to analyze multiple measurements (e.g. different preparations, different mutations) following the same protocol simultaneously, while linking parameters between datasets that are expected to be conserved, i.e. global analysis of PAM fluorometry data. In this way it is possible to more reliably quantify differences in photosynthetic efficiency or stoichiometry of the photosynthetic complexes between experiments. To illustrate this point, measurements on intact chloroplasts, prepared in a way that they were either devoid of zeaxanthin (V) or enriched in zeaxanthin (Z), are used as test cases throughout this paper.

Fig. 1 lists the different emissive species that may be encountered in this case. Each species is associated with a particular relative quantum yield Φ which will be estimated from the PAM quenching analysis curves. In the appendix it will also be demonstrated for the V and Z preparations how some of these quantum yields can also be independently estimated from picosecond time-resolved fluorescence measurements.

Thus our approach does take into account the biophysical origin of the emitting states which can interconvert, but describes the dynamics phenomenologically, i.e. with exponential decays. In the discussion we will close the loop, and connect to a theoretical model. The predictions from such a model can be quantitatively compared to the results from our parametric description, and thus inspire the iterative improvement of the theoretical model.

2. Materials and methods

The relevant paragraphs of the material and methods section from

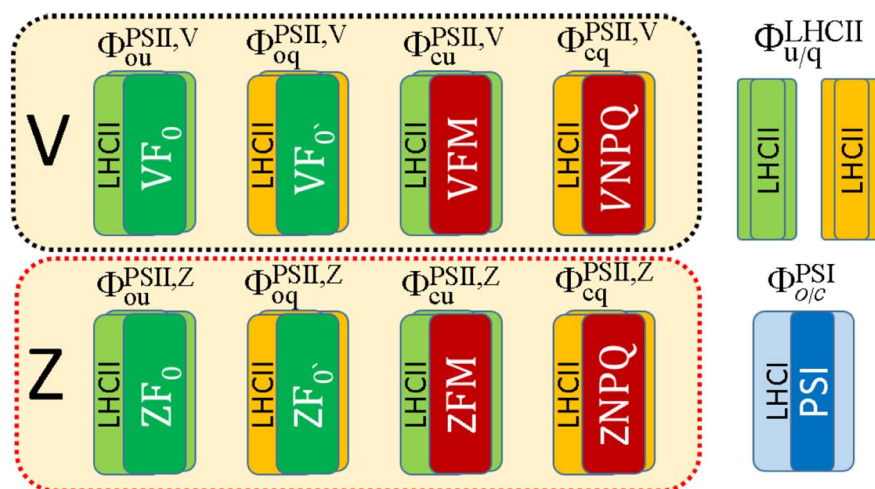


Fig. 1. Overview of the different emissive species that can contribute to a measured PAM curve for plants and green algae. The Photosystem II supercomplex can occur in four different states depending on whether the RC is open (o) or closed (c), and the complex as a whole is being quenched non-photochemically (q) or unquenched (u). The states are duplicated between the two different samples (V, Z) to emphasize that the yields may be different. Photosystem I can contribute but is assumed to be unaffected by quenching or saturating light conditions. Disconnected LHCII can also contribute and is assumed to be affected by quenching in the same way as PSII. Under normal conditions it is only present in negligible amounts.

[17] are reproduced below with minor modifications and clarifications.

2.1. Chloroplasts isolation

Spinach plants were grown for 8–9 weeks in Sanyo plant growth cabinets with an 8-h photoperiod at a light intensity of $250 \mu\text{mol of photons m}^{-2} \text{s}^{-1}$ and a day/night temperature of $22/18^\circ\text{C}$. Intact chloroplasts were prepared as described in [21]. Chloroplasts devoid of zeaxanthin and antheraxanthin (labeled -Zea or just V) were prepared from spinach leaves dark adapted for 1 h. Chloroplasts enriched in zeaxanthin (labeled +Zea or Z) were prepared from leaves pretreated for 30 min at $350 \mu\text{mol of photons m}^{-2} \text{s}^{-1}$ under 98% N_2 , 2% O_2 .

2.2. PAM fluorometry

Chlorophyll fluorescence was measured with a Dual-PAM-100 chlorophyll fluorescence photosynthesis analyzer (Heinz Walz) using the liquid cell adapter. Intact chloroplasts were measured in a quartz cuvette at a concentration of $12 \mu\text{M}$ chlorophyll under continuous stirring in the presence of $100 \mu\text{M}$ methyl viologen as a terminal electron acceptor. Actinic illumination ($350 \mu\text{mol of photons m}^{-2} \text{s}^{-1}$) was provided by arrays of 635 nm LEDs. F_o (the fluorescence level with PSII reaction centers open) was measured in the presence of a $10 \mu\text{mol of photons m}^{-2} \text{s}^{-1}$ measuring beam (fluorescence emitter: 620 nm (DUAL-DB)). The maximum fluorescence in the dark adapted state (F_m), during the course of actinic illumination (F_m') and in the subsequent dark relaxation periods was determined using a 0.8 s saturating light pulse ($4000 \mu\text{mol of photons m}^{-2} \text{s}^{-1}$). This is a standard protocol of applying saturating light pulses and the 0.8 s duration was chosen not to induce quenching, which was tested on dark-adapted samples subjected to pulses. The F_m level was found to be constant if 500–800 ms pulses were applied [22].

2.3. Time-resolved fluorescence spectroscopy

Time-correlated single photon counting measurements were performed using a FluoTime 200 ps fluorometer (PicoQuant). Fluorescence lifetime decay kinetics were measured on LHCII and intact chloroplasts ($4 \mu\text{M}$ chlorophyll) using excitation provided by a 470-nm laser diode using a 10 MHz repetition rate. These settings were carefully chosen to be far below the onset of singlet-singlet exciton annihilation ($< 0.1 \text{ pJ}$). Time-resolved emission spectra (TRES) were measured in the 655–760-nm detection region with 1-nm steps. The resolution of the time-to-amplitude converter was 4 ps/channel.

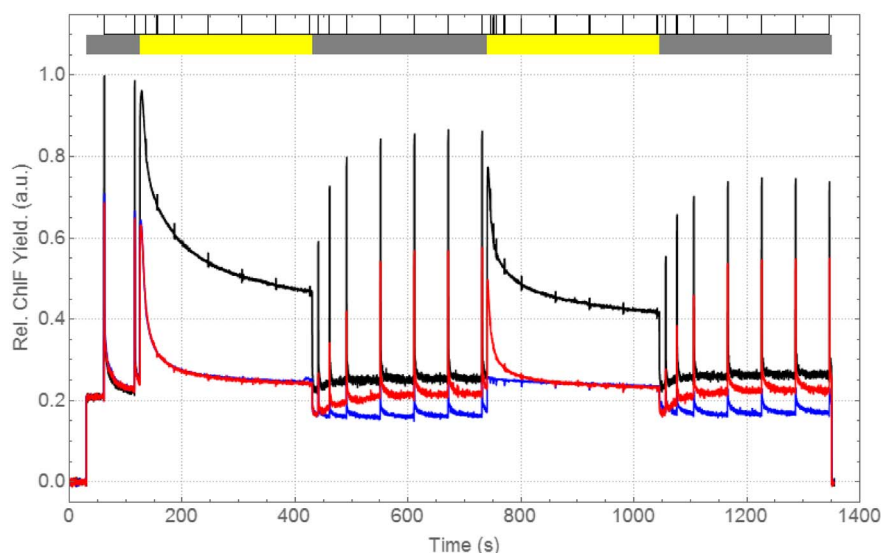


Fig. 2. PAM fluorescence quenching/induction curves obtained on intact Chloroplasts devoid of zeaxanthin (black), enriched in zeaxanthin (red, blue) using the saturating pulse method. Alternating darkness (dark adaptation, recovery, indicated by a gray bar above the curve) and continuous actinic light (inducing quenching, yellow bar) to measure quenching induction/recovery while periodically probing the maximal level of fluorescence with saturating pulses (indicated by stripes in the top of the graph). The blue curve represents a sample where glutaraldehyde was added (at $t \approx 410$ s) to prevent the recovery from the quenched state. Its peaks are obscured in this overlay figure, but are clearly visible in Fig. S7. The black curve was normalized to the maximum of the fluorescence in darkness, and the red and blue curves were then scaled to the minimal level of fluorescence in darkness of the black curve. Measuring light and actinic light of 620 and 635 nm respectively was used, and fluorescence was detected above 700 nm.

3. Experimental data

Fig. 2 shows three measured PAM fluorescence quenching curves obtained on dark adapted intact spinach chloroplasts either devoid (black curve) of, or enriched in zeaxanthin (red and blue curves), labeled respectively the “V”, “Z” and “GA” dataset. The relative chlorophyll fluorescence quantum yield is probed over a period of 25 min with 60 millisecond sampling intervals while subjected to a complex actinic light protocol controlling the actinic background light and saturating flashes. The GA dataset represented by the blue curve in Fig. 2 is similar to the Z dataset, except that around $t \approx 410$ s glutaraldehyde was added, largely inhibiting recovery of quenching. Glutaraldehyde, at the concentration used, stops NPQ recovery in the dark. Not only F_m' but also F_o' remains constantly in the quenched state. Delta-pH collapses though but judging by the stable PSII yield, the electron transport around PSII remains unaffected. The same data was presented in Fig. 1A of [17]. The light protocol can be used to distinguish a number of light regimes (LR0–LR6), indicated in the white/gray/yellow bar in Fig. 2. In the first 30 s (LR0: 0.02 s–30.02 s; white) a background signal is measured. Then the measuring light is switched on while the actinic light is still switched off (LR1: 30.08 s–124.94 s; gray), probing the minimal variable fluorescence level in the dark, typically labeled F_o and associated with completely open PSII RCs. Periodically a saturating pulse of light (0.8 s; $4000 \mu\text{mol m}^{-2} \text{s}^{-1}$) is applied (indicated by a black stripe on top of the bar in Fig. 2) probing the maximal level of variable fluorescence, typically labeled F_m when the sample is dark adapted, and labeled F_m' while the sample is exposed to actinic light, and associated with completely closed RCs. During the initial period of darkness two such saturating pulses are applied and some recovery dynamics following the saturating pulse is observed. The next phase of the experiment consists of a period of actinic light (level = $350 \mu\text{mol @ 635 nm}$) (LR2: 125.0–429.98; yellow) in which fluorescence quenching in the form of a steady decline of the fluorescence yield is observed, followed by a period of darkness (LR3: 429.98–740.0; gray) where the fluorescence (partially) recovers to the levels of the dark adapted state. A second period of actinic light (LR4: 740.06–1045.1; yellow) is again followed by a period of darkness (LR5: 1045.16 s–1350.02 s; gray) showing somewhat different dynamics, before the measurement light is again switched off (LR6: 1350.08 s–1354.94 s, white). Thus, the whole measurement can be divided into a number of discrete segments starting at the moment of a change in light conditions (measuring light on or off, actinic light on or off, saturating pulse on or off) and ending the moment in time just before another change is observed. For these data this amounts to 77 unique segments. The beginning of each

segment can be determined from the data by visual inspection, it can be estimated during the analysis, or, ideally, it can be automatically generated from the experimental protocol that was used to record the data. In each segment the data are fitted with a unique model function defined with respect to the start of the segment (time zero; t_0), while all model functions share a common parameter set.

4. Constructing a parametric model

To create a parametric description of our experimental data, we start by recognizing that the experimental data is the result of a PAM fluorometer running a complex light protocol while sampling the fluorescence quantum yield with high resolution. The protocol specifies exactly when and for how long the sample is exposed to a certain intensity (ranging from high to none) of actinic light and additionally when and for how long saturating flashes are given. The signal that is measured depends on the stoichiometry of the species probed with the PAM measuring light, as well as their specific quantum yield which, in the case of PSII, can strongly depend on the actinic light conditions. While the sum of concentrations of species may be constant, their stoichiometry certainly isn't. In this case study we consider four states of PSII: it can be open or closed and it can be part of a quenched or unquenched complex (see Fig. 1). PSII is considered closed when the Q_A site is reduced. We will return to the consequence of ignoring the PSI contribution in the discussion. Fig. 3 summarizes the method of analysis of PAM curves using a parametric model, subsequently every aspect will be discussed in more detail.

In order to construct a parametric model that can be used to fit and quantitatively describe PAM fluorometry curves the following assumptions are made. 1) The total fluorescence quantum yield can be described as the linear combination of the concentrations of a number of emissive species c^j and their quantum yields ϕ^j . 2) The quantum yields of these species are independent of their relative concentration or experimental (lighting) conditions.

A species is then defined as a pigment-protein complex which can be excited by the measuring light of the PAM fluorometer and which has a unique spectral and kinetic signature of excited state decay resulting in a specific contribution to the emission in the integration window of the PAM fluorometer (see also Fig. 1). The concentrations of the different species can change dynamically when one species is interconverted into another, in which case the sum of the concentrations can be assumed to remain constant. For instance if the process of closing PSII RCs by applying a saturating pulse can be described with $f(t)$ the concentration of open PSII is described with $(1-f(t))$. With high light exposure species

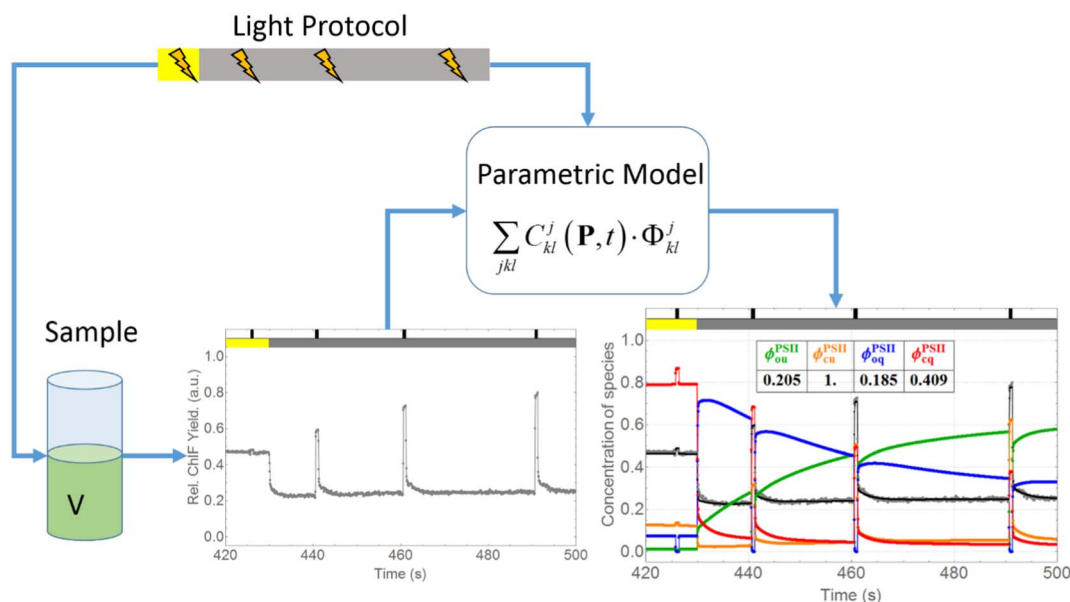


Fig. 3. PAM analysis method using a parametric model. A sample (of in this case intact chloroplasts devoid of zeaxanthin) is measured following a specific light protocol consisting of regimes of quenching inducing continuous actinic light, recovery regimes with no actinic light, and saturating pulses throughout the experiment. The resulting data as well as the light protocol form the input for a parametric model which results in a description of the data in terms of a number of species concentrations c^j and their quantum yields ϕ^j .

could get photoinactivated, leading to the photoinhibition of PSII activity. The dynamics of the concentrations as a function of the measurement time C_t is dependent on the light conditions of the experiment and can be parameterized with a parameter vector \mathbf{P} , which is independent of the species specific quantum yield Φ .

The total PAM signal J , decomposed into j species, can then be written as:

$$J^x(\mathbf{C}_t(\mathbf{P}); \Phi) = \sum_{jkl} c_{kl}^{j,x}(\mathbf{P}, t) \cdot \Phi_{kl}^{j,x} \quad (1)$$

where the additional indices k and l represent different light-acclimated states; e.g. in the case of PSII k takes into account whether the state is open or closed and l stands for either a quenched or an unquenched species. The label x is used to represent the state of zeaxanthin enrichment, e.g. V in the case of a sample devoid in zeaxanthin and Z in the case of the sample enriched in zeaxanthin. Enumerating over all species j for state x (where x equals V or Z) we get:

$$J^x = c_{ou}^{PSII,x} \cdot \Phi_{ou}^{PSII,x} + c_{cu}^{PSII,x} \cdot \Phi_{cu}^{PSII,x} + c_{oq}^{PSII,x} \cdot \Phi_{oq}^{PSII,x} + c_{cq}^{PSII,x} \cdot \Phi_{cq}^{PSII,x} \quad (2)$$

Taking the assumption of a limited number of discrete states (Fig. 1) substituted into a parametric model (Eq. (1) and Fig. 3) resulting in Eq. (2) we arrive at our working model depicted in Fig. 4. Here the dynamics of the concentrations $c_{ou}^{PSII,x}$, $c_{cu}^{PSII,x}$, $c_{oq}^{PSII,x}$, $c_{cq}^{PSII,x}$ is captured by a limited number of rate constants (k_1 , k_2 , etc), reflecting the interconversion of one state in the system to another. For instance k_1 (in a saturating pulse) or k_{10} (under actinic light) reflect the rates in which open unquenched PSII is converted to closed unquenched PSII, subsequently k_4 , k_{4a} and k_5 reflect the three rate constants needed to describe the quenching of PSII under the continued influence of actinic light (indicated by a red arrow). Returning to darkness the re-opening of the RC is described by k_2 , k_3 and k_{3b} and the recovery from quenching by rates k_8 and k_{8a} which occur in the absence of light as indicated by the blue arrows.

The amplitude fractions (how much decay can be ascribed to a particular rate constant) have been omitted from the figures for the sake of brevity, but are discussed below. Detailed considerations are described in the SI, section “Components of a parametric model for PAM curves”, which also lists the complete set of equations used for the total fitting function. To simplify the model, we assume that the

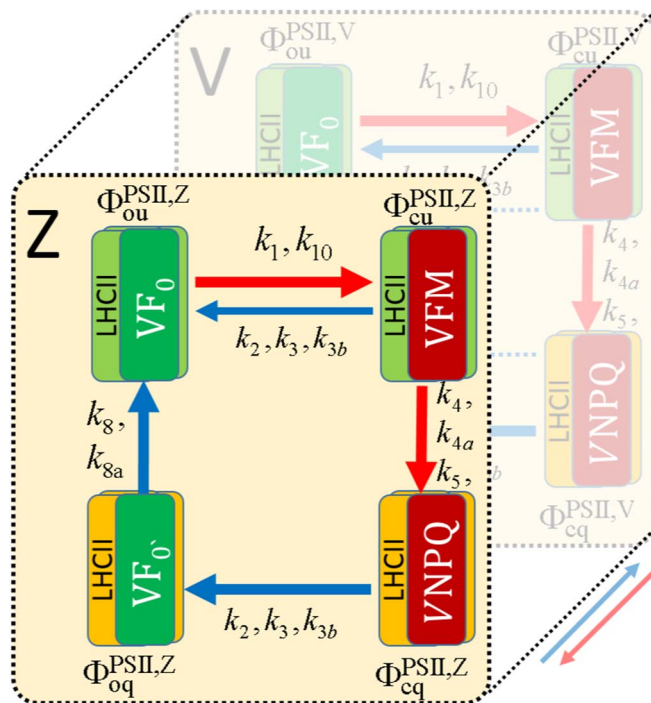


Fig. 4. Working mathematical model which ties the different species listed in Fig. 1 to the parametric description given in Eq. (2). The premise of the model are four distinct states which can be interconverted into one another with certain rates, either light driven (red arrows) or spontaneously in the absence of light (blue arrows). To simplify the model it was assumed that during the course of the experiment the concentration of zeaxanthin remains constant so that species only interconvert within the front plane defined by a certain fixed level of zeaxanthin.

concentration of zeaxanthin remains constant throughout the course of the experiment, as adding this complexity would add a third dimension to the model whereas the fitting results show that given the short duration of the experiments this extra complexity is not needed to adequately describe the data.

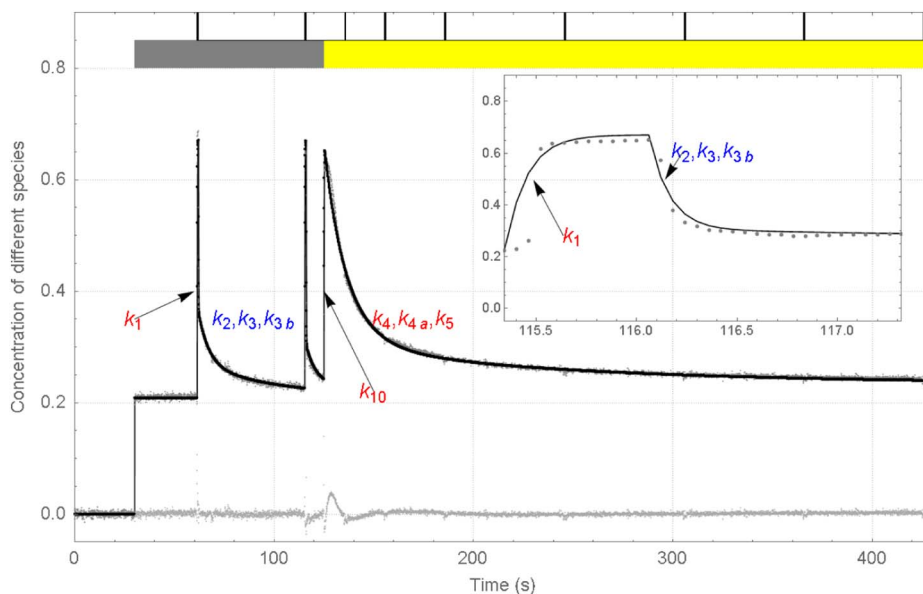


Fig. 5. Simulated PAM curve of intact spinach chloroplasts enriched in zeaxanthin. Legend: data (gray), simulation (black), residual (light gray, straddling the zero line). The bottom half of the color bar indicates the light condition (white: no ML, gray: only ML, yellow: ML and actinic light). The upper half indicates when a SP was applied. The inset represents a zoom of the second saturating pulse in darkness. The inset labels indicate which of the rates k_i from Fig. 4 apply to which segments in the data. Further details are discussed in the text.

5. Simulating PAM fluorometry curves

Using the function definition of Eq. (2) the quenching analysis curves can either be simulated using any chosen set of parameters or fitted directly to the measured data from Fig. 2. To illustrate the different aspects of the model, a simulation is performed with parameters which are in good agreement with those needed to describe the measurements of zeaxanthin enriched chloroplasts (red curve, Fig. 2). See Fig. S2 for an impression of the implementation of the simulation. Note that in the screenshot the contributions from species other than PSII (e.g. PSI) have been set to zero in this simulation. The first part of the simulation consists of a brief period of darkness, with two saturating pulses, and then a period of quenching inducing high light; this is shown in Fig. 5. The recovery period that follows the period of continuous actinic light is shown in Fig. 6. For comparison the measured data is shown by gray dots and the simulated trace in solid black. The residuals, defined as data minus simulation, are shown in light gray. Given the noise level of the data (standard deviation is < 0.01) it is clear from the residuals of this simulation that the model is not perfect but all essential features of the data are captured, which will be discussed below.

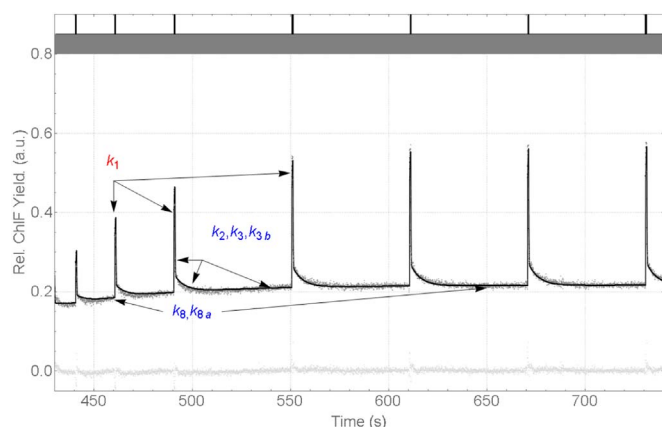


Fig. 6. Simulated PAM curve representing the recovery region following a period of actinic light as in Fig. 5. The simulated trace is in solid black, the observations are represented by dark gray dots. In light gray dots (straddling the zero line) are the residuals. The inset labels indicate which of the rates from Fig. 4 apply to which segments in the data.

The simulation starts with 30 s of background signal (ML off). When the ML is turned on (but the actinic light is still off), the signal instantaneously (in less than the 60 ms step size) reaches a level of minimal variable fluorescence, which can be written as the product of a time dependent (but in this case constant) concentration function and a constant quantum yield (the same throughout the simulation): $J = c_{ou}^{PSII}(t) \cdot \Phi_{ou}^{PSII}$ (where ou indicates that the RC is open and the complex as a whole is unquenched), with in this case $c_{ou}^{PSII}(t) = 1$, $\Phi_{ou}^{PSII} = 0.21$. Note that this quantum yield is not absolute but relative to the chosen normalization in Fig. 2. During this period of relative darkness (only ML) at two moments in time ($t_{SP1} = 61.40$; $t_{SP2} = 115.34$) a saturating pulse of about 0.8 s is applied, which is assumed to quickly close all PSII RCs, but not induce any quenching. This translates to a full conversion of the concentration of open unquenched PSII to closed unquenched PSII. The expression that captures this can be written as:

$$J = e^{-k_1(t-t_0)} \cdot \Phi_{ou}^{PSII} + (1 - e^{-k_1(t-t_0)}) \cdot \Phi_{cu}^{PSII} \quad \text{where } k_1 = 9.4s^{-1}, \Phi_{ou}^{PSII} = 0.21 \text{ as before, } \Phi_{cu}^{PSII} = 0.67 \text{ and where in lieu of } t_0 \text{ either } t_{SP1} \text{ or } t_{SP2} \text{ is substituted. After the saturating pulse the subsequent reopening of the closed PSII RCs is modeled using a sum of three exponentials that describes the conversion of closed unquenched PSII back into open unquenched PSII.}$$

$$J = (1 - c_{cl}^{PSII}(t)) \cdot \Phi_{ou}^{PSII} + c_{cl}^{PSII}(t) \cdot \Phi_{cu}^{PSII} \quad \text{with } c_{cl}^{PSII}(t) = a_2 e^{-k_2 D^1(t-t_0)} + a_3 e^{-k_3(t-t_0)} + a_{3b} e^{-k_{3b}(t-t_0)}$$

where $k_2 = 9.4s^{-1}$, $k_3 = 0.002s^{-1}$, $k_{3b} = 0.16s^{-1}$, $a_2 = 0.65$, $a_3 = 0.06$, $a_{3b} = 0.29$ for SP1 and $a_2 = 0.81$, $a_3 = 0.03$, $a_{3b} = 0.16$ for SP2. The recovery after the very first saturating pulse in darkness is slower than that after subsequent saturating pulses.

Following the period of relative darkness, as indicated by the gray bar in Fig. 3, is a period of continuous actinic light, indicated by a yellow bar. The moment the actinic light is switched on (t_{LR2}) the fluorescence level is observed to rise due to the closing of all PSII RCs, which is again approximated with a single exponential rise. However, the maximum level of fluorescence yield reached is somewhat lower than during the saturating pulses in darkness, which is modelled here by the immediate onset of a fast quenching process. This means that at this point all states of PSII as illustrated in Fig. 1 can occur simultaneously. For simplicity we only describe the contribution of PSII in the closed and quenched state, by far the dominant component during the period of actinic light, which can be written as the product of a closing function and a quenching function times the relevant quantum yield:

Table 1

Parameter values estimated using non-linear regression. Four quantum yields, sixteen rate constants and ten fractional amplitude parameters are given. For more information on the nature of each parameter the reader is referred to **Table S1** and the corresponding section in the SI. The relation between the fractional amplitude parameters and the amplitude parameters reported in the main text is given in **Table S2**. Parameters fixed during regression are indicated in bold. Parameters that were not relevant for a given case are marked with '–'. The value of k_8^{R1} listed for the Z + GA case applies to the Z dataset only, for the GA dataset it was fixed to 0 (there is no recovery from quenching in this case).

	$\Phi_{\text{oc}}^{\text{PSII}}$	$\Phi_{\text{cu}}^{\text{PSII}}$	$\Phi_{\text{cq}}^{\text{PSII}}$	$\Phi_{\text{cu}}^{\text{PSII}}$	k_1^{D1}	k_1^{H1}	k_{10}^{H1}	k_2^{D1}	k_{3b}^{D1}	k_3^{D1}
V	0.185	0.205	0.409	1.000	20	20	9.3	16	0.41	0.0441
Z	0.152	0.209	0.234	0.671	9.5	–	11	9.9	0.19	0.0238
GA	0.159	0.207	0.231	0.701	9.4	–	24	9.5	0.16	0.021
Z + GA	0.162	0.209	0.233	0.684	9.5	–	13	9.8	0.19	0.0244

	k_2^{H1}	k_4^{H1}	$k_{\text{SQ}}^{\text{H1}}$	k_5^{H1}	k_4^{H2}	k_5^{H2}	k_6^{H1}	k_6^{H2}	k_8^{R1}	k_{8a}^{R1}
V	35	0.050	0.0041	0.132	0.14	0.02	0.027	k_6^{H1}	0.038	0.0002
Z	–	0.008	0.061	0.105	0.02	0.21	–	–	0.020	0.0005
GA	–	0.089	0.0052	0.1	–	–	–	–	0	0.0005
Z + GA	–	0.006	0.048	0.12	0.02	0.20	–	–	0.019	0.0002

	$f_{\text{rcc}}^{\text{H1}}$	$f_{\text{rSQ}}^{\text{H1}}$	f_{r}^{D1}	$f_{\text{r3b}}^{\text{D1}}$	$f_{\text{r}}^{\text{SP1}}$	$f_{\text{r3b}}^{\text{SP1}}$	f_{r}^{R2}	$f_{\text{r3b}}^{\text{R2}}$	f_{r}^{H1}	f_{r}^{H2}
V	0.91	0.46	0.81	0.53	0.78	0.54	0.75	0.52	0.77	0.78
Z	1.00	0.27	0.79	0.73	0.66	0.62	0.75	0.64	0.22	0.24
GA	1.00	0.14	0.81	0.73	0.66	0.65	0.39	0.80	0.93	0.24
Z + GA	1.00	0.28	0.80	0.75	0.66	0.62	0.73	0.68	0.18	0.24

$$J_{\text{cq}}^{\text{PSII}} = \overbrace{(cl_D + (1 - cl_D)(1 - e^{-k_{10}(t-t_0)}))}^{\text{closing}} \underbrace{((1 - f_{\text{rSQ}}e^{-k_{\text{SQ}}(t-t_{\text{PLR}})} - (1 - f_{\text{rSQ}})(a_4e^{-k_4(t-t_{\text{PLR}})} + (1 - a_4)e^{-k_5(t-t_{\text{PLR}})}))\Phi_{\text{cq}}^{\text{PSII}}}_{\text{quenching}}$$

Here $cl_D = 0.09$ represents a fraction of the total PSII population which is (still) closed, due to the remaining effect of a preceding saturating pulse, and defined as the function c_{cl}^{PSII} evaluated at the last time point in darkness. The conversion of PSII in the open state to the closed state occurs with a rate of $k_{10} = 10/\text{s}$, and t_0 is substituted with the start of the actinic light regime ($t_{\text{LR2}} = 125 \text{ s}$). Quenching is divided into two fractions which differ in their rate of recovery. A slow-to-recover quenching fraction $f_{\text{rSQ}} = 0.27$ rises with a rate $k_{\text{SQ}} = 0.07 \text{ s}^{-1}$. A quick-to-recover fraction $(1 - f_{\text{rSQ}}) = 0.73$ rises on two timescales, a small fraction $a_4 = 0.22$ rises relatively slowly with a rate of $k_4 = 0.01/\text{s}$ and a fraction $(1 - a_4) = 0.78$ rises with rate $k_5 = 0.1/\text{s}$. The full expression can be found in the SI, but in principle it is easily derived since the concentration of PSII in the open state is $(1 - \text{closed})$, and the amount of unquenched PSII is $(1 - \text{quenched})$. The full expression also takes into account that a fraction of the PSII re-opens during the course of actinic light illumination, when the excitation pressure from the actinic light is not enough to keep all PSII RCs closed. In this simulation it is assumed that all RCs are continually closed ($f_{\text{rcc}} = 1$, see SI) during actinic light because of the absence of a fluorescence increase upon a saturating pulse during the period of actinic light.

After a period of actinic light follows a period of darkness during which the sample can recover from quenching as shown in **Fig. 6**. The initial effect of switching from actinic light to relative darkness is re-opening of the PSII RCs, exactly as would happen after a saturating pulse. Then on a longer timescale the sample also recovers from the quenching induced by the actinic light, a fraction recovering quickly and the rest so slowly that at the end of the recovery period a large part of it still hasn't recovered, as can be observed in **Fig. 2**. For simplicity we describe here only the contribution of PSII in the open unquenched state, which describes the baseline level during a recovery period. Again the other contributions can easily be derived from this expression but for the complete expression the reader is referred to the SI. The contribution of PSII in the open and unquenched state to the total PAM signal J during recovery then becomes:

$$J_{\text{ou}}^{\text{PSII}} = \overbrace{(a_2(1 - e^{-k_2(t-t_0)}) + a_3(1 - e^{-k_3(t-t_0)}) + a_{3b}(1 - e^{-k_{3b}(t-t_0)}))}^{\text{opening}} \left(\overbrace{(1 - f_{\text{rSQ}})(1 - QT_f + (1 - e^{-k_8(t-t_{\text{PLR}})})QT_f)}^{\text{fast recovery}} + \overbrace{f_{\text{rSQ}}(1 - QT_s + (1 - e^{-k_{8a}(t-t_{\text{PLR}})})QT_s)}^{\text{slow recovery}} \right) \Phi_{\text{ou}}^{\text{PSII}}$$

where $k_2 = 9.4\text{s}^{-1}$, $k_3 = 0.16\text{s}^{-1}$, $k_{3b} = 0.002\text{s}^{-1}$, $a_2 = 0.81$, $a_3 = 0.13$, $a_{3b} = 0.06$, $f_{\text{rSQ}} = 0.27$. The variables QT_f and QT_s represent how much quenching was induced during the preceding period of actinic light for the fast-to-recover fraction and the slow-to-recover fraction respectively. In this simulation $QT_f \approx 1$, $QT_s \approx 1$. The rates $k_8 = 0.02/\text{s}$ and $k_{8a} \approx 1/\text{h}$ are the rates of recovery for the fast and slow fraction respectively. The parameters a_2 , k_2 , a_3 , k_3 , a_{3b} , k_{3b} , in principle are linked between the initial period of darkness and the period of recovery, meaning that the dynamics of re-opening, following a saturating pulse in darkness or actinic light, or the re-opening after switching off the actinic light, is treated in the same way.

In general linking the parameters between the different segments is an a priori assumption that fits well, however in the case that the dynamics are clearly observed to be different, additional labeled parameters can be introduced, e.g. k_2^{R1} where the label R1 indicates that the parameter is defined specifically for the first recovery regime. In the same way D1 can be used for the first period of darkness, H1 for the first period of actinic light, H2 for the second, etc.

The values of the estimated parameters, i.e. four estimated quantum yields, sixteen rate constants and ten amplitude fractions are collated in **Table 1**. Thus with the help of our parametric model we have successfully extracted ≈ 30 parameters from each PAM trace that consisted of 22,583 data points.

6. Calculating derived quantities

With a completely parameterized description of the PAM curve in place, it is possible to calculate derived quantities such as the commonly used NPQ parameter (see **Fig. S3**) however the interpretation of this quantity and especially the fitting thereof is not without controversy [23]. Thus, it is more interesting to directly visualize the individual contribution of each species (or in this case, each state of PSII) to the total signal. This decomposition is visualized for the Z dataset in

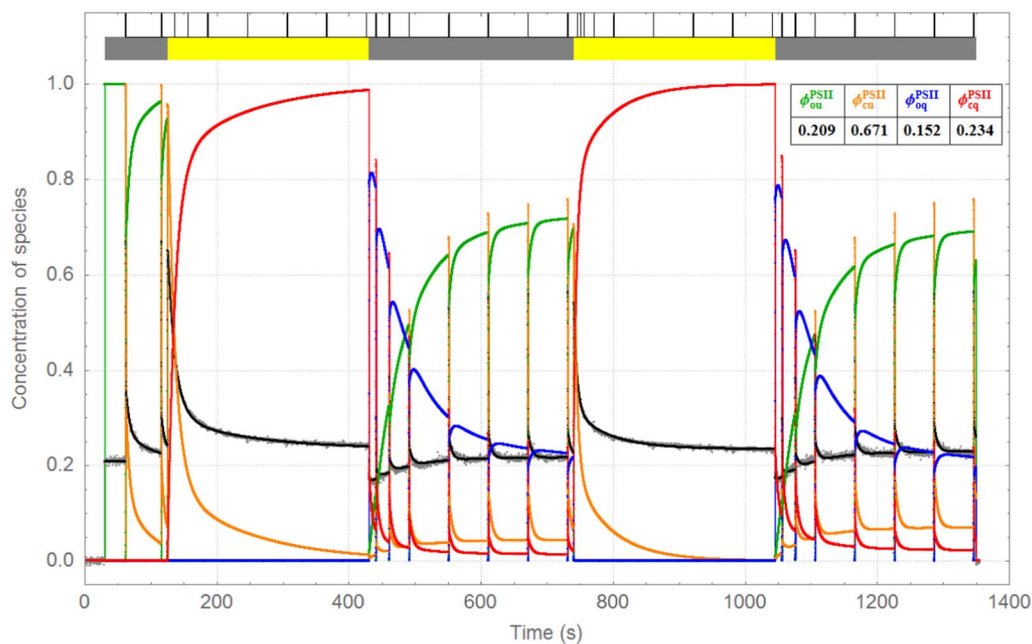


Fig. 7. Concentration profiles of the different states of PSII contributing to the total relative chlorophyll fluorescence quantum yield for the Z dataset. The sum of the concentrations, open unquenched PSII (green, $\Phi_{\text{ou}}^{\text{PSII}} = 0.209$), closed unquenched PSII (orange, $\Phi_{\text{cu}}^{\text{PSII}} = 0.671$), open quenched PSII (blue, $\Phi_{\text{oq}}^{\text{PSII}} = 0.152$) and closed quenched PSII (red, $\Phi_{\text{cq}}^{\text{PSII}} = 0.234$) multiplied by their respective quantum yields result in the fitted PAM curve depicted in solid black. For comparison the Z observations are overlaid as gray dots. Light conditions are indicated by the top bar as described in the caption of Fig. 2.

Fig. 7 and **Fig. S5**. In **Fig. 7** the concentrations of the four different states of PSII are shown as a function of the measurement time, at any given moment summing up to a total concentration of 1. In **Fig. S5** the contribution of each state to the total quantum yield (overlaid in gray dots, maximum 0.69) is shown. The black curve represents the sum over the product of concentration and quantum yield for all four states (see table inset).

In the beginning, the contribution of PSII open unquenched (green curve) is maximal. At the first saturating pulse this concentration drops to zero and the contribution of PSII in the closed unquenched state (depicted in orange) is maximal. After the saturation pulse is completed (0.8 s after the onset) the concentration of closed unquenched decays back into open unquenched. Just before the next saturating pulse the level is still not yet at the level of F_0 in darkness indicating that a small fraction ($\approx 5\%$) is still closed. When the actinic light is switched on (indicated by a yellow bar) the concentration of PSII closed quenched is observed to quickly rise (red curve) at the expense of the closed unquenched state. After switching the actinic light off again the fourth species enters, open quenched PSII (blue curve). The lowest level in the data (well below F_0 in darkness) largely determines $\Phi_{\text{oq}}^{\text{PSII}}$. During the recovery from quenching the quenched concentrations (red/blue) are gradually replaced by unquenched (orange/green), but not completely. A substantial amount ($\approx 20\%$) of open quenched PSII (blue) remains, even after 300 s of recovery. This is a direct consequence of the observation in the data (cf. the red curve in **Fig. 2**) that the level of F_m' at the end of the recovery period is substantially lower than F_m in darkness. The same holds true for the maximum level reached upon turning on the actinic light after the first recovery period. This accumulation of a slow-to-recover quencher is described by the remaining concentration in the blue curve. But despite this incomplete recovery from quenching, the baseline level of fluorescence in the data is even slightly higher than the level of F_0 in the initial period of darkness. Considering that the yield of open quenched PSII lies below that of open unquenched PSII, there has to be a certain fraction of closed quenched and closed unquenched PSII left which is seen as a non-zero amplitude of the red and orange curves toward the end of the recovery periods. This permanently closed fraction visible in **Fig. 7** is 7% after the first recovery period, and 11% after the second period of actinic light. This effect is even more clearly visible in the decomposition of the V dataset, shown in **Fig. 8** (concentrations) and **Fig. S6** (contributions), where the baseline level of F_0 following a period of recovery is substantially higher than during the

initial period of darkness, and the accumulation of the slow-to-recover quencher and the fraction of permanently closed PSII is even more pronounced. Here the permanent closed fraction is 8% after the first recovery period, 17% after the second recovery period.

The main difference between **Figs. 7** and **8** is the re-opening of a small fraction of PSII RCs during actinic light. This is directly observed in the data as well: during actinic light upon application of a saturating pulse the observed yield is slightly higher still. This is now visualized in **Fig. 8** as the blue concentration, which slowly rises (it is assumed that the initial switching on of the actinic light first closes everything) and which drops to zero every time a saturating pulse is applied. As a consequence the concentration of red/orange features a small spike which lasts only for the duration that the saturating pulse is applied. In contrast to the period of darkness and recovery, where the actinic light is on, the decay of the extra closed concentration is extremely fast under the influence of actinic light. Another relevant difference is that the quenching level reached after the second period of actinic light is substantially lower than after the first period, which is explained by a quenched fraction which takes longer to form and is slow-to-recover.

The decomposition of the GA dataset is shown in **Fig. S4** (concentrations) and **Fig. S7** (contributions).

7. Fitting PAM curves

Instead of mimicking the data by adjusting the parameters by hand, the parameters can also be estimated using any non-linear regression method. The implementation in this paper was constructed in Wolfram Mathematica, but the expression could easily be ported to any other language or platform which has non-linear solvers available, such as Matlab, Python, R or C++.

Fig. 9 shows the fitted PAM curves for the V and Z datasets following optimization of the parameters using non-linear regression. The V data is plotted in gray dots, the fit in solid black, and the residual light gray. The Z data is shown in orange dots, the fit in solid red and the residuals in dark gray.

Not all parameters were set to be free parameters of the fit. In the case of the V dataset the quantum yield of PSII in the closed unquenched state is fixed to 1 by definition, since the data was normalized to the maximum of the first saturating pulse, where the only contribution is assumed to be closed unquenched PSII. In the Z dataset, because the saturating pulses during actinic light don't result in an

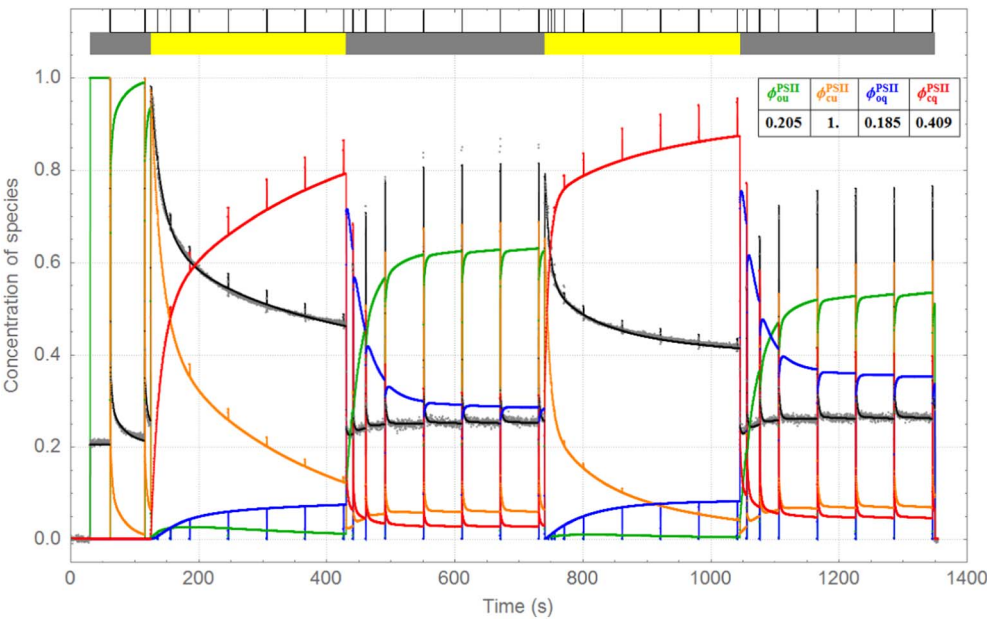


Fig. 8. Concentration profiles of the different states of PSII contributing to the total relative chlorophyll fluorescence quantum yield for the V dataset. The sum of the concentrations, open unquenched PSII (green, $\phi_{\text{ou}}^{\text{PSII}} = 0.205$), closed unquenched PSII (orange, $\phi_{\text{cu}}^{\text{PSII}} = 1.0$), open quenched PSII (blue, $\phi_{\text{oq}}^{\text{PSII}} = 0.185$) and closed quenched PSII (red, $\phi_{\text{cq}}^{\text{PSII}} = 0.409$) multiplied by their respective quantum yields produce the PAM curve depicted in solid black. For comparison the V observations are overlaid as gray dots. Light conditions are indicated by the top bar as described in the caption of Fig. 2.

increased yield, the parameter relating to the amount of continuously closed PSII in actinic light (f_{CC}) was fixed to 1, which automatically means that the rate constant related to partial re-opening (k_6) could be eliminated from the list of parameters to be optimized. Instead in the V dataset the fraction was a free parameter of the fit and could be fitted ($f_{\text{CC}} = 0.9$), and the rate of partial re-opening was found to be $k_6 = 0.03\text{ s}^{-1}$. In addition it was found that the fraction of slow-to-recover quenching ($f_{\text{SQ}}^{\text{H1}}$) was found to be substantially larger in the V dataset (0.46) than in the Z dataset (0.27) (see Table 1). It is this large value of $f_{\text{SQ}}^{\text{H1}}$ which explains the relatively large difference between Fm during the initial phase of darkness (1.0) and Fm' at the end of the second recovery phase (Fm' = 0.75), and at least partially the difference between Fm' at the end of the second and the first period of recovery (Fm' = 0.85). Recently, a similar slow to recover quenching effect was attributed to plant 'memory' [16], although there it was primarily related to the accumulation of zeaxanthin.

In Fig. 9, the parameters for the V and Z dataset were optimized for each dataset separately, but the real power of having a parameterized description of the PAM curve is when multiple datasets are analyzed with a shared set of parameters, i.e. global analysis of PAM fluorometry

data. A straightforward application is when several repeats of a specific protocol are measured on the same sample. Rather than averaging the repeated measurements, they could all be analyzed with a single model with a shared set of parameters. These parameters can thus be estimated more precisely. A more interesting example is to link parameters between different experiments, for instance in the case of the Z dataset, and the GA dataset, which are very similar up to the point where glutaraldehyde is added to the sample in the GA dataset to prevent recovery. To fit both datasets simultaneously a new model function is defined where all parameters are linked between both datasets, except for the rate of recovery for the slow- and fast-to-recover fractions. The rate of fast-to-recover quenching k_8 is set to zero for the GA dataset, whereas the rate of slow-to-recover quenching k_{8a} is a free parameter of the fit.

Fig. 10 shows the results of the linked analysis of the Z and GA datasets. Looking at the fitted curves and the residuals in Fig. 10 it is clear that a small price is paid by linking all but one model parameter (k_8 , the rate of fast recovery), but overall both datasets are described well with this single model with linked parameters. As more parameters are unlinked (thereby increasing the number of free parameters) the fit

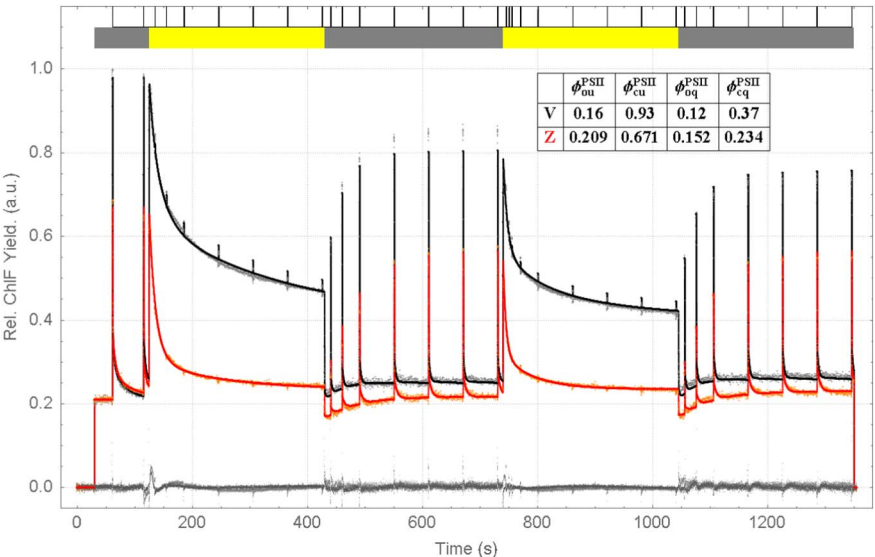


Fig. 9. Fitted PAM curves for the V and Z dataset where non-linear regression was used to estimate the parameters (estimated values in Table 1). Estimated relative quantum yields (relative to $\phi_{\text{cu}}^{\text{PSII}, V} = 1$) collated in the inset table. Data, fit and residuals (straddling the zero line) for the V and Z dataset respectively shown in: gray dots, solid black, light gray dots, and orange dots, solid red and dark gray dots. Light conditions indicated by the top bar as described in the caption of Fig. 2.

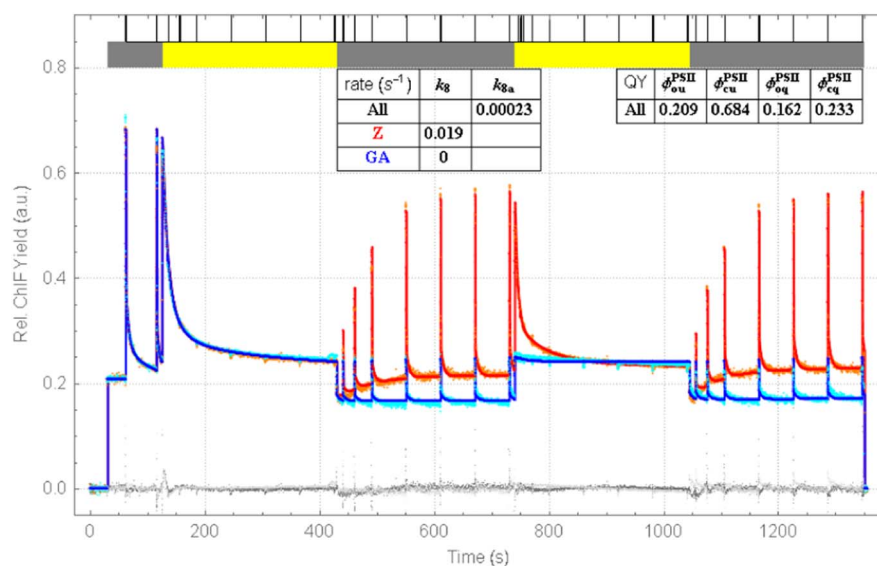


Fig. 10. Simultaneous linked analysis of the Z and GA datasets. The Z data is shown in orange dots, the fit in solid red and the residuals in dark gray. The GA data is plotted in cyan dots, the fit in solid blue, and the residuals in light gray. All model parameters between the two datasets are linked and shown in Table 1 except for the rates of slow and fast recovery (shown in the left table inset). The quantum yields estimated from the linked analysis are shown in the right table inset.

can improve. Judging from the values in Table 1 it can also be observed that the linked parameters related to quenching resemble those estimated when fitting the Z dataset alone. For instance the parameter for the fraction of slow quenching (f_{SQ}^{HI}) is estimated to be 0.27 for the Z dataset, 0.14 for the GA dataset, but 0.28 for the Z + GA linked analysis. Thus the Z dataset contributes relatively more information in the linked fit.

8. Discussion

The key assumption made in this paper is that the fluorescence quantum yield as measured by PAM fluorometry can be described by the sum of a number of discrete molecular states, each with their own fluorescence quantum yield. This assumption derives from the extensive study of photosynthetic samples using time-resolved fluorescence spectroscopy where it can be shown that the observed fluorescence can also be decomposed in the contributions by different complexes [24] facilitated by sophisticated target analysis [25]. We demonstrate that the quantum yields estimated from the analysis of the PAM data are consistent with the quantum yields estimated from ultra-fast time-resolved fluorescence spectroscopy data, see Table S4 in the Supporting Information section “The link with time-resolved fluorescence spectroscopy”. The fact that our model can describe the data without any detachment of the LHCII antenna from PSII is in agreement with the claims of recently published experimental work [26]. Using millisecond fluorescence induction of dark adapted intact chloroplasts [26] discovered that NPQ does not decrease the rate of the transition from F_0 to F_m state upon illumination – evidence that the functional antenna size did not decrease in the NPQ state.

Our modelling enabled to assess the amount of photoinactivation based upon the levels of F_0 and F_0' . This assessment is entirely consistent with the recently proposed methodology of the determination of the photoprotective effectiveness of NPQ [27,28]. This photoinactivation assessment methodology uses the relationship between the PSII yield and NPQ as well as compares the measured level of F_0' and the theoretically predicted F_0' . The parametric model also uses the level of F_0' to calculate the fraction of the damaged PSII RCs.

Although PSI is part of our parametric model specification and its quantum yield is also estimated in the time-resolved measurements, we have chosen not to include it in the main text/figures for two reasons: (1) PSI contributes only a constant offset as its quantum yield is not significantly affected by the actinic light conditions, therefore it will not affect the estimated dynamics and (2) the results from our analysis of time-resolved fluorescence show the contribution of PSI to be rather

small, on the order of 4% of F_m or 20% at F_0 (given 475 nm excitation, assuming 1:1 stoichiometry of PSII:PSI). This justifies neglecting the contribution of PSI in first approximation if we're only interested in comparing the relative effect in PSII, but it does signify the importance of a parametric model based analysis which can account for the influence of PSI when it is needed, especially considering the effect on the estimated relative quantum yields. The resulting decomposition including PSI is shown in Fig. S8 (concentrations) and Fig. S9 (contributions).

Another strong assumption that we have made is that the number of species stays constant throughout the measurement, especially with respect to the sample devoid of zeaxanthin (V sample). In reality the chloroplasts in this sample might accumulate some zeaxanthin throughout the measurement, which has recently been demonstrated to function as a short-term light memory in plants [16]. This would imply that the population dynamics of PSII would have to be modelled with a total of eight species (present in the inset table of Fig. 9). This would be in agreement with the so called four state two site quenching description of PSII [16,29], which attributes the fast induced quenching to a mechanism driven by the pH sensing protein PsbS and the slower quenching to the formation of zeaxanthin [21,30,31]. However, despite our simplification to only four states for PSII per measurement, we have demonstrated an overall good agreement with the data.

In order to facilitate the comparison between our approach and the theoretical model by Matuszyńska et al. we have used our light protocol in their simulation code and generated a comparable decomposition (see Fig. S12). In their model Matuszyńska et al. take into account a fraction of open and closed PSII and a total level of quenching dependent on the relative concentrations of PsBs and Zeaxanthin. This amounts to a gradually increasing level of quenching of all PSII RC's, rather than a gradual population switch between unquenched and quenched centers as is the case in our model. The comparison between our V dataset and the prediction of Fig. S12 shows that although there is reasonable qualitative agreement much of the dynamics is not yet captured. The analysis of Fig. 8 can inspire the iterative improvement of the theoretical model. In particular, a fraction of slowly recovering closed unquenched seems necessary to describe the F_0' deviations in Fig. S12.

Fluorescence quenching analysis by means of PAM fluorometry is a useful tool to study NPQ in different samples under a wide variety of physiologically relevant conditions. In one experiment the information about the condition of the sample before illumination, during quenching inducing continuous actinic light and during recovery can be obtained (Fig. 2). Underlying the fluorescence quantum yield measured

by the PAM fluorometer are the contributions from a number of different emissive species, summarized in Fig. 1 for the case of plants. Each species corresponds to a pigment-protein complex with its own concentration and its own absorption and emission signature for the combination of excitation by the PAM instrument measuring light and its detection window. This simple observation is enough to then formulate Eq. (1) which states that the observed PAM signal can be parametrized as the sum of a number of species' concentrations multiplied by their quantum yields (Fig. 3). Even for a typical PAM analysis quenching experiment as depicted in Fig. 2, the concentration function can get complicated rather quickly, because the concentration of each species is not only dependent on the light conditions at time t , but also on the light conditions at all times prior to this. By segmenting the dataset based on changes in the light condition experienced by the sample, either due to the presence or absence of measuring light or the presence or absence of actinic light, and observing which segments preceded, it becomes possible to describe the dynamics for each segment with a limited number of functions (see Table S1). In principle the segmentation can be entirely automated if the PAM measurement protocol is known, although the start and end time point for each segment can also be determined empirically from the data, either by manual inspection or by fitting it. Each function is composed of a number of basis functions from a so called Basis Function Set as detailed in the section "Components of a parametric model for the PAM curves" in the SI. For this paper the aim was to keep the function description as simple as possible, so all concentration dynamics is essentially described by a number of exponential functions (for the rise and decay) and a constant term (to reflect the transitional effects). For instance the closing of PSII RCs due to the application of a saturating pulse is modelled by a single exponential rise (thus the concentration of open PSII RCs, defined as one minus the concentration of closed PSII RCs is modeled by a single exponential decay). From the inset of Fig. 5 it can be seen that this is not a perfect description of the observed rise, but it captures the trend and more importantly the starting and end concentration are modelled correctly. It is known from the literature that this fluorescence induction dynamics is much more complex than can be captured by a single exponential rise, and many papers have been published that model this dynamics in great detail (e.g. [32,33], reviewed in [34,35]). It was shown that when data is obtained at a higher time-resolution at least 3 exponentials are needed [6,36], in which case it would be worthwhile to extend the Basis Function Set to capture this dynamics, but for the datasets used in this work only 13 data points are observed during a saturating pulse and a single exponential sufficed. Overall it can be seen from Figs. 5 and 6 that with the limited set of functions described in Table S1 the data can be mimicked quite accurately. Of course with a full parameterized description of the PAM curve it is also possible to gain more insight in the closing and quenching dynamics by overlaying the data with the concentration profiles of the individual species as shown in Fig. 7; the sum of the products of the quantum yields (inset) and their concentrations then reproduce the observed PAM fluorescence quantum yield (cf. Eq. (1)). A parameterized description allows for the use of standard non-linear regression to estimate the parameters from the data as is demonstrated in Fig. 9 for the V and Z datasets. But the real power of a parametrized description is revealed when multiple datasets are fitted simultaneously with a common set of parameters. The simplest application of this is when instead of averaging several measurements on the same sample, the measurements are analyzed with a single model resulting in statistically relevant quantities with a meaningful standard deviation. This can be done *even* when there is a small shift in the exact time of the saturating pulses or of the moment of switching on the actinic light between measurements, which would significantly distort the averaged data. A more advanced application is shown in Fig. 10 where the Z and the GA measurements, with at first sight completely different dynamics, are simultaneously fitted with a common set of parameters and only a single free parameter between the two datasets. In this way the

hypothesis of what exactly happens to the quenching dynamics upon the addition of glutaraldehyde can be more rigorously tested. The fitted parameters obtained by fitting each dataset individually, as well as the parameters obtained in the combined fit, are listed in Table 1. These results demonstrate that the analysis of a single PAM fluorometry quenching experiment can already provide information on the relative quantum yield of the four different states of PSII for the intact chloroplasts. To the best of our knowledge no other form of spectroscopy provides this information in a single measurement.

Transparency document

The <http://dx.doi.org/10.1016/j.bbabo.2017.08.004> associated with this article can be found, in online version.

Acknowledgments

This research is performed as part of the BioSolar Cells research programme, sponsored by the Dutch Ministry of Economic Affairs. IHMV and RvG acknowledge financial support of the European Research Council (Advanced Grant Proposal 267333 (PHOTPROT) to RvG). RvG gratefully acknowledges his Academy Professor grant from the Netherlands Royal Academy of Sciences (KNAW). AVR acknowledges the Leverhulme Trust grant RPG-2012-478 and UK Biotechnology and Biological Sciences Research Council grant BB/L019027/1. AVR would like to acknowledge The Royal Society for the Wolfson Research Merit Award and the NWO visiting scholarship grant 040.11.433. MPJ would like to acknowledge the Leverhulme Trust grant ECF-2012-398\2. JM Gruber and LW Bielczynski are thanked for helpful discussions regarding the interpretation of the modeling.

Appendix A. Supplementary data

Supplementary data to this article can be found online at <http://dx.doi.org/10.1016/j.bbabo.2017.08.004>.

References

- [1] A.V. Ruban, Nonphotochemical chlorophyll fluorescence quenching: mechanism and effectiveness in protecting plants from photodamage, *Plant Physiol.* 170 (2016) 1903–1916.
- [2] J. Kromdijk, K. Glowacka, L. Leonelli, S.T. Gabilly, M. Iwai, K.K. Niyogi, S.P. Long, Improving photosynthesis and crop productivity by accelerating recovery from photoprotection, *Science* 354 (2016) 857–861.
- [3] U. Schreiber, Pulse-amplitude modulation (PAM) fluorometry and saturation pulse method: an overview, *Chlorophyll a Fluorescence: A Signature of Photosynthesis*, 2004, pp. 279–319.
- [4] U. Schreiber, U. Schliwa, W. Bilger, Continuous recording of photochemical and non-photochemical chlorophyll fluorescence quenching with a new type of modulation fluorometer, *Photosynth. Res.* 10 (1986) 51–62.
- [5] W. Bilger, U. Schreiber, M. Bock, Determination of the quantum efficiency of photosystem II and of non-photochemical quenching of chlorophyll fluorescence in the field, *Oecologia* 102 (1995) 425–432.
- [6] W.J. Vredenberg, A three-state model for energy trapping and chlorophyll fluorescence in photosystem II incorporating radical pair recombination, *Biophys. J.* 79 (2000) 26–38.
- [7] R.J. Ritchie, Fitting light saturation curves measured using modulated fluorometry, *Photosynth. Res.* 96 (2008) 201–215.
- [8] G. Schansker, S.Z. Tóth, L. Kovács, A.R. Holzwarth, G. Garab, et al., *Biochim. Biophys. Acta Bioenerg.* 1807 (2011) 1032–1043.
- [9] D. Lázár, G. Schansker, Models of chlorophyll a fluorescence transients, *Photosynth. Silico* 29 (2009) 85–123.
- [10] A. Rubin, G. Riznichenko, Govindjee, Modeling of the primary processes in a photosynthetic membrane, in: A. Laisk, L. Nedbal (Eds.), *Photosynthesis In Silico: Understanding Complexity from Molecules to Ecosystems*, Springer, Netherlands, 2009, pp. 151–176.
- [11] N. Belyaeva, A. Bulychiev, G.Y. Riznichenko, A. Rubin, Thylakoid membrane model of the Chl a fluorescence transient and P700 induction kinetics in plant leaves, *Photosynth. Res.* (2016) 1–25.
- [12] O. Ebenhöf, T. Houwaart, H. Lokstein, S. Schlede, K. Tirok, A minimal mathematical model of nonphotochemical quenching of chlorophyll fluorescence, *Biosystems* 103 (2011) 196–204.
- [13] J. Zaks, K. Amarnath, D.M. Kramer, K.K. Niyogi, G.R. Fleming, A kinetic model of rapidly reversible nonphotochemical quenching, *Proc. Natl. Acad. Sci.* 109 (2012)

- 15757–15762.
- [14] O. Ebenhöf, G. Fucile, G. Finazzi, J.-D. Rochaix, M. Goldschmidt-Clermont, Short-term acclimation of the photosynthetic electron transfer chain to changing light: a mathematical model, *Philos. Trans. R. Soc. Lond. B Biol. Sci.* 369 (2014) 20130223.
 - [15] A. Matuszyńska, O. Ebenhöf, A reductionist approach to model photosynthetic self-regulation in eukaryotes in response to light, *Biochem. Soc. Trans.* 43 (2015) 1133–1139.
 - [16] A. Matuszyńska, S. Heidari, P. Jahns, O. Ebenhöf, A mathematical model of non-photochemical quenching to study short-term light memory in plants, *Biochim. Biophys. Acta Bioenerg.* 1857 (2016) 1860–1869.
 - [17] M.P. Johnson, A.V. Ruban, Photoprotective energy dissipation in higher plants involves alteration of the excited state energy of the emitting chlorophyll(s) in the light harvesting antenna II (LHCII), *J. Biol. Chem.* 284 (2009) 23592–23601.
 - [18] R.B. Peterson, V. Oja, H. Eichelmann, I. Bichele, L. Dall'Osto, A. Laisk, Fluorescence F_0 of photosystems II and I in developing C_3 and C_4 leaves, and implications on regulation of excitation balance, *Photosynth. Res.* 122 (2014) 41–56.
 - [19] G. Schansker, S.Z. Tóth, R.J. Strasser, Methylviologen and dibromothymoquinone treatments of pea leaves reveal the role of photosystem I in the Chl a fluorescence rise OJIP, *Biochim. Biophys. Acta Bioenerg.* 1706 (2005) 250–261.
 - [20] E. Belgio, M.P. Johnson, S. Jurić, A.V. Ruban, Higher plant photosystem II light-harvesting antenna, not the reaction center, determines the excited-state lifetime—both the maximum and the nonphotochemically quenched, *Biophys. J.* 102 (2012) 2761–2771.
 - [21] S. Crouchman, A. Ruban, P. Horton, PsbS enhances nonphotochemical fluorescence quenching in the absence of zeaxanthin, *FEBS Lett.* 580 (2006) 2053–2058.
 - [22] M.P. Johnson, A. Zia, A.V. Ruban, Elevated ΔpH restores rapidly reversible photoprotective energy dissipation in *Arabidopsis* chloroplasts deficient in lutein and xanthophyll cycle activity, *Planta* 235 (2012) 193–204.
 - [23] A.R. Holzwarth, D. Lenk, P. Jahns, On the analysis of non-photochemical chlorophyll fluorescence quenching curves: I. Theoretical considerations, *Biochim. Biophys. Acta* 1827 (2013) 786–792.
 - [24] J.J. Snellenburg, L.M. Włodarczyk, J.P. Dekker, R. van Grondelle, I.H. van Stokkum, A model for the 77K excited state dynamics in *Chlamydomonas reinhardtii* in state 1 and state 2, *Biochim. Biophys. Acta Bioenerg.* (2016).
 - [25] I.H.M. van Stokkum, D.S. Larsen, R. van Grondelle, Global and target analysis of time-resolved spectra, *Biochim. Biophys. Acta* 1657 (2004) 82–104.
 - [26] E. Belgio, E. Kapitonova, J. Chmeliov, C.D.P. Duffy, P. Ungerer, L. Valkunas, A.V. Ruban, Economic photoprotection in photosystem II that retains a complete light-harvesting system with slow energy traps, *Nat. Commun.* 5 (2014) 4433.
 - [27] A.V. Ruban, E. Belgio, The relationship between maximum tolerated light intensity and photoprotective energy dissipation in the photosynthetic antenna: chloroplast gains and losses, *Philos. Trans. R. Soc. B Biol. Sci.* 369 (2014).
 - [28] A.V. Ruban, Quantifying the efficiency of photoprotection, *Philos. Trans. R. Soc. Lond. B* (2017), <http://dx.doi.org/10.1098/rstb.2016.0393> (in press).
 - [29] A.R. Holzwarth, Y. Miloslavina, M. Nilkens, P. Jahns, Identification of two quenching sites active in the regulation of photosynthetic light-harvesting studied by time-resolved fluorescence, *Chem. Phys. Lett.* 483 (2009) 262–267.
 - [30] A.Z. Kiss, A.V. Ruban, P. Horton, The PsbS protein controls the organization of the photosystem II antenna in higher plant thylakoid membranes, *J. Biol. Chem.* 283 (2008) 3972–3978.
 - [31] X.-P. Li, A.M. Gilmore, S. Caffarri, R. Bassi, T. Golan, D. Kramer, K.K. Niyogi, Regulation of photosynthetic light harvesting involves intrathylakoid lumen pH sensing by the PsbS protein, *J. Biol. Chem.* 279 (2004) 22866–22874.
 - [32] D. Lázár, Chlorophyll a fluorescence rise induced by high light illumination of dark-adapted plant tissue studied by means of a model of photosystem II and considering photosystem II heterogeneity, *J. Theor. Biol.* 220 (2003) 469–503.
 - [33] X.G. Zhu, Govindjee, N.R. Baker, E. de Sturler, D.R. Ort, S.P. Long, Chlorophyll a fluorescence induction kinetics in leaves predicted from a model describing each discrete step of excitation energy and electron transfer associated with photosystem II, *Planta* 223 (2005) 114–133.
 - [34] A. Stirbet, Govindjee, Chlorophyll a fluorescence induction: a personal perspective of the thermal phase, the J-I-P rise, *Photosynth. Res.* 113 (2012) 15–61.
 - [35] H.M. Kalaji, V. Goltsev, M. Brestic, K. Bosa, S.I. Allakhverdiev, R.J. Strasser, Govindjee, In Vivo Measurements of Light Emission in Plants, (2014), pp. 69–96.
 - [36] D. Joly, R. Carpentier, Sigmoidal reduction kinetics of the photosystem II acceptor side in intact photosynthetic materials during fluorescence induction, *Photochem. Photobiol. Sci.* 8 (2009) 167–173.